Applied Catalysis B: Environmental 195 (2016) 39–47

Contents lists available at ScienceDirect

Applied Catalysis B: Environmental

journal homepage: www.elsevier.com/locate/apcatb

The amorphous phase in titania and its influence on photocatalytic properties

V.A. Lebedev[a], D.A. Kozlov[a], I.V. Kolesnik[a], A.S. Poluboyarinov[a], A.E. Becerikli[b], W. Grünert[b], A.V. Garshev[a,c,*]

[a] Faculty of Materials Science, Lomonosov Moscow State University, Moscow, Russia
[b] Laboratory of Industrial Chemistry, Ruhr-University Bochum, Bochum, Germany
[c] Baikov Institute of Metallurgy and Material Science RAS, Moscow, Russia

ARTICLE INFO

Article history:
Received 15 February 2016
Received in revised form 29 April 2016
Accepted 3 May 2016
Available online 7 May 2016

Keywords:
Titania
Crystallinity
Amorphous titania
Photocatalytic activity
XRD

ABSTRACT

In the present work, we compare the photocatalytic activity (PCA) of titania samples normalized to the sample weight and specific surface area (SSA), and show a correlation between the PCA of titania catalysts with similar phase compositions and amorphous phase contents. In our studies, we used the commercial samples, P25 Evonik (formerly Degussa), Hombikat UV100, and pre-synthesized mesoporous titania. Catalysts with a significant amorphous content were annealed and processed by partial dissolution in acid and included in the analysis. PCA was measured by methyl orange (MO) photodegradation in an aqueous catalyst suspension under high-pressure Hg bulb illumination and the pH was controlled using phosphate buffer (pH 6.9). The weight percentage of the amorphous phase was determined using reference intensity ratios (RIR) for X-ray diffraction patterns of the titania samples measured with crystalline silicon additives. The reproducibility of the proposed method was demonstrated by measuring the amorphous content in mixtures of the sample and XRD-amorphous titania. The contributions of amorphous titanium oxohydroxides $TiO_{2-0.5n}(OH)_n \cdot xH_2O$ and water physically adsorbed to the amorphous phases were distinguished by thermogravimetric analysis. The obtained results show that the PCA of the titania samples decreases with the weight percentage of the amorphous phase, as low as 5% of the PCA of P25 in the case of $\omega_{Am}(TiO_2) > 25\,\%$. It was demonstrated that the partial removal of the amorphous phase by annealing or dissolution in nitric acid leads to a significant increase of PCA.

1. Introduction

The photochemical properties of titania are extensively studied due to its use in many practical applications, such as air and water purification, solar cell production, and water photolysis [1]. The following characteristics of titanium dioxide are usually considered key factors that lead to high photocatalytic activity (PCA) [1,2]: high surface area [3], high concentration of surface hydroxyls [4–7], optimal particle size [8–11], and high crystallinity [3,12–14].

The particle surface area is one of the key factors affecting PCA because photocatalytic processes on semiconductors are heterogeneous by nature and involve the surfaces of photocatalysts. On the other hand, high surface area is usually associated with low crystallinity and a high concentration of defects. The current data on the PCA of TiO_2 with a high surface area are controversial. It was demonstrated in [3] that TiO_2 with a specific surface area (SSA) of 230 m^2/g has a higher PCA than commercially available TiO_2 (P25, 50 m^2/g). In contrast, commercially available pure anatase Hombikat UV100 with an SSA of >300 m^2/g shows significantly lower PCA than P25 [15], despite its higher SSA.

The TiO_2 photocatalyst with a higher surface area may have a lower PCA for the following reason. In a few articles it was demonstrated that P25 has high crystallinity (<15% of XRD-amorphous phase) [16,17], whereas Hombikat UV100 has a significant amount of XRD-amorphous phase and a complicated microstructure [15]. Therefore, the differences in PCA may be explained by variations in the amorphous phase content. According to the literature, the amorphous phase is not photocatalytically active because of its high concentration of structural defects [1,12,18]. Only one exception from this trend was found [19]; but in this particular case, PCA was measured in the presence of strong acids. Therefore, the amorphous component would have had no impact on the PCA if it was dissolved.

* Corresponding author at: Faculty of Materials Science, Lomonosov Moscow State University, 119991 Moscow, Russia.
E-mail address: garshev@inorg.chem.msu.ru (A.V. Garshev).

http://dx.doi.org/10.1016/j.apcatb.2016.05.010
0926-3373/

Thus, when comparing the PCA of different samples, ignoring the amorphous phase content can lead to contradictory results. However, the number of methods for analyzing the amorphous phase is limited because of its complicated atomic structure. Some methods may be useful for analysis of the amorphous phase: transmission electron microscopy (TEM), X-ray diffraction [15], nuclear magnetic resonance [20], Mössbauer spectroscopy [21], Raman spectroscopy [22,23], and electron paramagnetic resonance, especially with temporal resolution [24]. Determination of the local spatial distribution is more complicated, but possible with the aid of TEM [25], High-resolution (HR)-TEM, and electron energy loss spectroscopy (EELS) in scanning transmission electron microscopy (STEM) mode [26]. However, quantification of the amorphous titania causes some difficulties. The usual approach is to determine its weight. There are several ways to do this: without intrinsic standards (using the intensity ratio between the halo and peaks) or with standard additives (100%-crystalline or 100%-amorphous) and the analysis of peak intensities based on the reference intensity ratios (RIRs). Methods without additional standards involve halo intensity estimation, and are applicable only in the case of a high (>90%) quantity of the amorphous phase [27]. Therefore, for common titania-based catalysts, only methods with standard additives can be applied. As a crystalline standard, one can use NiO [16], $CaCO_3$ [13], CaF_2 [15], α-Al_2O_3 [17], rutile [28], or any crystalline substance with a suitable RIR and weak peak interferences. From this point of view, the use of pure corundum does not seem to be a good option for anatase-based samples because of the overlapping intensive peaks at 25.5° and 37.8°. Typical errors introduced during the measurements may be caused by poor pre-weighing, sample mixing, or XRD-profile fitting. Using the RIRs-based methods, one obtains results with an accuracy of about 10–15%. Therefore, without reducing errors, this method should be used very carefully.

Petkov et al. [29] suggest that the amorphous phase contains an irregular assembly of short, staggered chains of octahedral [TiO_6] units, as in the brookite structure. According to Zhang et al. [30], the amorphous phase present in TiO_2 powders obtained by the hydrolysis of titanium alkoxide consists of 2 nm primary particles. They have a strained anatase-like core with two crystalline unit cells of anatase and a highly distorted shell. The average coordination number of Ti is 5.3 due to the truncation of the Ti-O octahedra in comparison with bulk anatase, rutile, and brookite structures. In several quantum chemical calculations, the authors used [TiO_x] models containing polyhedra with different coordination numbers of Ti, and the resulting average coordination number of Ti varied from 5 to 6 [31–33].

Thus, amorphous titanium oxide has a complicated structure that may contain different [TiO_x] polyhedra. The structure is disordered but may contain structural fragments in which the type of titanium-oxygen octahedral connection is similar to that in the anatase or brookite structure. On the other hand, amorphous and partially crystalline gels synthesized via hydrolysis of alkoxides or inorganic salts may contain several types of OH-groups formed during olation and oxolation of the precursor [34]. The vertices and edges of [TiO_x] polyhedra may also be decorated by hydroxyls, and water molecules may be physically adsorbed on the surface of the amorphous phase as well.

Therefore, using X-ray based methods to measure the amorphous phase content, one can describe the XRD-amorphous phase as amorphous titanium oxohydroxide $TiO_{2-0,5n}(OH)_n \cdot xH_2O$, however, physically adsorbed water may be present as well. It is necessary to use thermogravimetry data to discriminate these contributions [13].

The aim of the present study was to develop a method for precise quantitative analysis of the amorphous phase content in TiO_2 photocatalysts, and to determine the impact on its PCA in aqueous suspensions. The study was performed using different titania samples, before and after crystallization processing.

2. Experimental

2.1. Materials

Powdered polycrystalline silicon with a particle size of <50 μm was used as a 100%-crystalline standard for XRD measurements. Commercial titania samples, such as Evonik (formerly Degussa) Aeroxide® P25 and Hombikat UV100, were used without modification. Titanium tetrabutoxide (TBT) $Ti(O^nBu)_4$ (97%, Aldrich 244112), Pluronic P123 (typical molar weight 5800 g/mol, Aldrich 435465), 1 M standard HCl solution (Aldrich 38282), and deionized water (Milli-Q, Millipore) were used for the synthesis of mesoporous titania. Nitric acid, used for processing, was distilled in a *DistillAcid*™ (Berghof, Germany) system. Hydrophosphate-dihydrophosphate solution was used as a pH buffer (pH 6.9).

2.2. Synthesis

Mesoporous titania ($mTiO_2$) with a high SSA and tunable phase composition was synthesized by the template method [35] using Pluronic P123 as a surfactant during TBT acid hydrolysis (pH 2). After hydrolysis, the freshly obtained titania was washed three times with deionized water (DI) and once with ethanol to remove the major part of the surfactant. Finally, we calcined the obtained sample for 12 h at 350 °C under synthetic air flow to remove remnants of the organics and to obtain crystalline TiO_2. According to Zhang [28], such annealing leads to a crystallinity of >90%.

Amorphous titania was obtained via hydrolysis of TBT in a water–ethanol mixture [36,37], then washed in water and dried at 60 °C. The absence of organics in the resulting titania was confirmed by infrared (IR) spectroscopy.

2.3. Characterization

The sample microstructure was characterized using scanning electron microscopy (SEM, Zeiss Leo Supra 50VP) and transmission electron microscopy (TEM, Zeiss Libra 200). The collected images were processed with open-source software Gwyddion [38].

X-ray diffraction (XRD) patterns were collected using a Rigaku D/MAX 2500 diffractometer ($\theta/2\theta$ Bragg-Brentano reflection geometry) with a scintillation counter. All the measurements were performed with $CuK_{\tilde{\alpha}}$ radiation generated on a rotating Cu anode (40 kV, 250 mA) and monochromatized by a curved graphite [0 0 2] monochromator placed at the reflected beam. The incidence beam path included a 1/2° divergence slit, the diffracted beam – a 1/2° scatter slit, 0.3 mm receiving slit, and 2.5° Soller slit. For precise phase analysis, the XRD patterns were obtained in the 3–90°2θ range with a 0.02° step and at least 10 s/step. For the full profile analysis, the XRD patterns were obtained in the 20–90°2θ range with a 0.01° step and at least 2 s/step. To reduce the undesirable background intensity, we used low-background monocrystalline Si sample holders oriented by [5 1 0] for all measurements.

Thermogravimetric experiments were performed on a simultaneous thermogravimetric analyzer (STA 409 PC Luxx, Netzsch, Germany) with a heating rate of 2 °C/min up to 1000 °C in air.

The nitrogen sorption isotherms for multipoint Brunauer–Emmett–Teller (BET) analysis and Barrett–Joyner–Halenda (BJH) calculations were obtained at 77 K using a Quantachrome Nova 2400e instrument. Prior to the measurements, the samples were evacuated for 6 h at 200 °C.

2.4. Methods

2.4.1. Photocatalytic activity measurements

The PCA was measured through the decoloration of methyl orange (MO, $C_14H_14N_3NaO_3S$) in aqueous solutions under UV illumination. As we aimed for a uniform illumination of the reaction mixture, we used a cylindrical quartz IceGlass® reactor with a contour thermostat and a high-pressure Hg bulb (5 W) inside. There were no additional light filters used to prepare the pure UV illumination, but the PCA of TiO_2 under the visible part of this illumination is extremely low in the case of our setup [39].

To reduce the influence of temperature changes on the reaction rate during the experiment, all measurements were performed with a coolant temperature of 40 °C. The pH value was stabilized with phosphate buffer solution (pH 6.9) during the decoloration process. For each measurement, ~3 mg of sample was used, corresponding to a TiO_2 concentration of ~0.2 g/L in the reaction mixture. The MO concentration in the mixture was 47 mg/L.

To perform measurements with high temporal resolution, the suspension containing the photocatalyst and MO was circulated through a transparent U-shaped cuvette throughout the photodegradation process.

Absorbance spectra were measured every few seconds with a Xenon lamp HPX-2000 and an OceanOptics QE65000 spectrometer. Spectra processing was performed using the original *Python 2.7* software. It evaluated the time dependency of the spectra maxima in the 330–700 nm range with respect to a background, which was simultaneously calculated for each spectrum as the mean intensity in the range of 650–700 nm, where the intensity of MO and titania extinction are low.

On the obtained curves, selected points corresponding to the stabilization of catalyst suspensions and to turning the lamp on were selected. We found that under these experimental conditions, the titania powder suspensions were stable for at least 2–3 h, which is long enough to measure the MO decoloration rate. Finally, the software subtracted the spectrum of the stable catalyst mixture from all experimental spectra, calculated the time dependency of the maxima, and normalized the absorbance intensity of MO to the value corresponding to the concentration at the onset of illumination.

There are many works about the precise determination of MO photodegradation kinetics in the presence of titania, and it is well known that the order of this reaction is pseudo-first in the case of both direct and indirect oxidation [40–43]. Therefore, decoloration rates were calculated by the linear approximation of the relative concentration of MO against time in a semi-log scale. The calculated rates were normalized to the sample weight. Finally, to compare the measured rates of decoloration with the results of other groups, we defined the relative PCA of our samples by relating their MO decoloration rates of the sample (r_S) to that of P25 (r_{P25} =−0.035 1/(*h mg*)) measured under the same conditions:

$$PCA_m(S) = \frac{r_S/m_S}{r_{P25}/m_{P25}} \cdot 100\%, \quad (1)$$

$$PCA_{SA}(S) = PCA_m(S) \cdot \frac{SSA_{P25}}{SSA_S} \cdot 100\%, \quad (2)$$

where $PCA_{SA}(S)$ is the PCA of the sample, normalized to the surface area.

2.4.2. XRD pattern fitting

The ICDD PDF-2 base was used for phase identification. The RIRs were taken from different cards and averaged (Table 1). The preference was given to cards calculated from theoretical patterns because real titania samples (especially anatase and brookite) may contain some amount of the amorphous phase, which can impact the measured RIR.

Table 1
ICDD card numbers.

Phase	RIR	ICDD card
Silicon	4.7 ± 0.2	27-1402, 75-0589
Anatase	4.8 ± 0.5	71-1169, 78-2486, 84-1286
Brookite	1.6 ± 0.3	76-1934
Rutile	3.4 ± 0.2	21-1276, 72-1148, 73-1232

After phase analysis, the XRD profiles were fitted using the JANA2006 software [44]. We described the obtained background there as a Legendre polynomial and subtracted it. For peak fitting, we used a modified pseudo-Voigt function [45]. The peak asymmetry was calculated from the beam divergence using of the $H/L = S/L$ equation for geometry parameters (see [46] and JANA2006 cookbook for details). Fitting was performed without texture, roughness, or absorbance corrections. All XRD patterns were fitted to reduce the profiles and weighted R-factors (R_p and wR_p) to less than 10. The integral intensities of the fitted peaks were taken in order to measure the crystallinity. The average size of the coherent scatter region (CSR) was calculated from Lorentzian contributions, L_X, by the equation [45]:

$$CSR_{iso} = p_\perp = \frac{180 \cdot K \cdot \lambda}{\pi L_X}, \quad (3)$$

where K is the Scherrer constant.

The le Bail [47] method of profile analysis was used for integral intensity measurements for the majority of XRD patterns. The full Rietveld method, for the calculation of peak integral intensities, was applied only in the case of significant overlap between main peaks, as in the case of the anatase and brookite mixture, in which all intensive anatase peaks, e.g. [1 0 1], [1 0 3], [0 0 4], and [2 0 0], overlap with those of brookite [1 2 0], [2 0 1], [2 3 1], etc. In this case, we refined the profile and lattice parameters with fixed atomic positions for all phases.

2.4.3. Crystallinity measurements

The total amounts of amorphous phase in the titania samples were determined using a crystalline standard (Si) and amorphous titania. We mixed the titania sample to be investigated and the standards in different weight ratios, executed XRD experiments, then performed phase analysis, and measured the integral intensities of the main peaks by the le Bail method. For each phase, A_i, in the sample, the mean integral intensity, $I(\bar{A}_i)$, was calculated by averaging the strong peak, $\langle hkl_i \rangle$, intensities and normalizing to the theoretical intensities.

After that, we calculated the weight percentages of the crystalline phases, $\omega_{XRD}(A_i)$, for all mixtures with the use of RIRs (Table 1).

$$X_i = \frac{I(\bar{A}_i)}{RIR_i}, \quad \omega_{XRD}(A_i) = \frac{X_{A_i}}{\sum_j X_j} \cdot 100\% \quad (4)$$

The details of the calculations are provided in SI, ch. 1. It is noteworthy that $\omega_{XRD}(A_i)$, calculated by (4), corresponds to the percentage of the crystalline component of the A_i phase in the crystalline portion of the mixture.

2.4.4. Infrared spectroscopy

The vibrational bands of the OH-groups were studied by Fourier transform infrared spectroscopy (FTIR). Infrared diffuse reflectance spectra were recorded using a Perkin Elmer Spectrum One FTIR spectrometer with a Specac Selector diffuse reflectance accessory. No dilution of the samples was performed prior to the

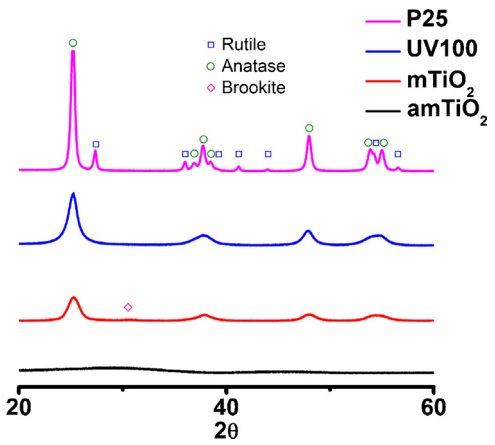

Fig. 1. XRD patterns of source samples.

measurements. The spectra were recorded from 4000 to 1000 cm^{-1} with 32 sample scans and 2.0 cm^{-1} resolution.

3. Results and discussion

3.1. XRD phase analysis

The amorphous TiO_2 ($amTiO_2$) sample obtained by hydrolysis of TBT was characterized by powder XRD (Fig. 1). The absence of strong, sharp reflections of any crystalline phase is clearly observed, and only a weak, broad hump centered at 32° is present. The XRD pattern is very similar to the XRD pattern of XRD-amorphous TiO_2 reported in [30]. Given the absence of diffraction peaks in the XRD pattern of this sample, we used it as an additive to check the consistency of the proposed RIR-based method for amorphous phase quantification.

From the XRD data (Fig. 1), the mesoporous titania appears to consist of anatase with a small amount of brookite. To quantify this amount of brookite, it is necessary to use the Rietveld method and refine the XRD pattern with respect to crystalline structures of compounds because of the strong peak interference. The experimental, calculated, and differential patterns are shown in Fig. SI3.

According to the calculations, the normalized integral intensities of anatase and brookite are 108 ± 19 and 6 ± 1, respectively. Relying on these results and the RIRs from Table 1, we conclude that the crystalline part of mesoporous TiO_2 is composed of 87 ± 3 % anatase and 13 ± 3 % brookite. The obtained values are in good agreement with the theoretical phase volume calculated in JANA2006: 12.9% for brookite.

The mean coherent scattering regions (CSR) for all the source samples were calculated using eq. (3) and are shown in Table 2.

The crystalline part of the commercial samples, as expected, consists of pure anatase (UV100) and a rutile-anatase mixture (P25). The rutile to anatase weight ratio in P25 was calculated from the integral intensities obtained by profile fitting with respect to the RIRs. There is 14 ± 2 % rutile and 86 ± 2 % anatase in the crystalline part of TiO_2 P25, which agrees well with the data reported in [16]. The deviation from the well-known 20:80 ratio can be explained by variations in the actual P25 composition [15,16].

3.2. TEM data

TEM methods were used for direct observation of the amorphous and crystalline parts. In conventional TEM images, there are undoubtedly crystalline particles surrounded by a potentially amorphous substance (Fig. 2a and c). The size of the crystalline particles is in good agreement with the CSR size, but during the TEM measurements, the observable amount of the amorphous substance significantly decreases, which can be caused by crystallization under electron beam irradiation (Fig. 2b). To determine the crystallinity of this substance, dark-field images were collected in the conical regime with a centered objective aperture, while the incident beam was tilted and moved conically. This method allows visualization of all the crystalline particles that have a diffraction peak anywhere in the chosen interplanar distance range, not only in the selected angular area, as in the case of the conventional dark field. In the image obtained by this method with the anatase [1 0 1] peak selected (Fig. 2d), we can see bright areas corresponding to the crystalline particles, and a gray area that has been illuminated due to a low-intensive halo corresponding to the surrounding substance. By TEM data, a significant amount of amorphous phase is visible in the UV100 sample, which has low PCA despite its crystalline phase composition and high SSA. We can see that it is possible to use TEM methods for observation of the amorphous phase and its spatial distribution in the case of TiO_2, but there are a lot of complexities in quantifying the results due to the local character of this method and its impact on the sample.

3.3. Specific surface area of the samples

In order to compare all of the samples by their PCA, it is necessary to measure their SSA. For this aim, multipoint BET analysis of liquid nitrogen sorption was used. The obtained data are shown in Table 2. Sorption isotherms and pore size distributions calculated by the BJH model are plotted at Fig. SI4. In the basic approach, the SSA value is related to the particle size and, hence, the CSR size calculated for the crystalline samples. As expected, the data in Table 2 demonstrate that samples with a small CSR size, such as UV100 and $mTiO_2$, have a high SSA (300 m^2/g and 150 m^2/g, respectively). In contrast, P25 has a relative low SSA (40 m^2/g). It was shown that the synthesized titania is mesoporous and has a narrow pore size distribution with a maximum pore radius of 3.2 nm. However, since it was shown

Table 2
Crystalline phase composition, CSR, SSA, measured amount of amorphous phase, TG results, and PCA.

Sample	R:A:B[a],%	CSR,nm	*SSA*, m^2/g	PCA_m,%	ω_{Am}, %	Δm_{total}, %	Δm_{H_2O}, %	$\omega_{Am}TiO_2$,%
$amTiO_2$	–:–:–	–:–:–	250	0[b]	100	27	21.5	78.5
P25	14:86:– ±2	100:50:– ±5	40	100	14 ± 1	2.3	0.9	13 ± 2
UV100	–:100:–	–:8:– ±2	330	15	32 ± 2	11.2	6.5	25 ± 2
UV100ac	–:100:–	–:8:– ±2	280	75	32 ± 2	15.0	7.9	24 ± 2
UV100@400	–:100:–	–:18:– ±2	170	45	25 ± 2	6.3	3.0	22 ± 2
UV100@500	–:100:–	–:31:– ±3	130	42	20 ± 5	5.7	3.0	17 ± 5
$mTiO_2$	–:87:13 ±3	–:19:8 ± 2	160	5	30 ± 1	5.6	2.4	28 ± 1
$mTiO_2$ac	–:87:13 ± 3	–:20:6 ± 2	160	33	24 ± 2	6.5	2.7	24 ± 2
$mTiO_2$@400	–:87:13 ± 5	–:19:5 ± 2	110	60	23 ± 2	4.5	2.0	20 ± 2
$mTiO_2$@500	–:90:10 ± 5	–:25:6 ± 2	60	85	19 ± 2	2.8	0.9	18 ± 1

[a] R:A:B – rutile:anatase:brookite weight ratio in crystalline portion.
[b] Observed PCA is in the range of MO decoloration under UV without catalysts.

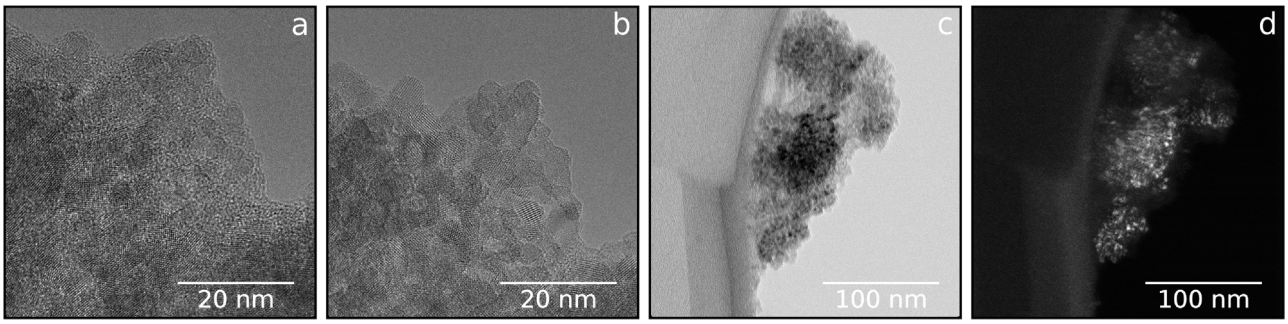

Fig. 2. (a) TEM, UV100 sample, (b) TEM from the same point after 30 min of irradiation, (c) bright field TEM, UV100, and (d) conical dark field TEM from the same point.

in [37] that the pore size distribution has a minor influence on the sorption processes in the case of titania, we did not focus on this parameter.

3.4. Precise quantification of amorphous phase using RIR-based method

As discussed, the composition of the crystalline component of titania-based catalysts is currently well studied. However, since a significant part of the TiO_2 sample may consist of the XRD-amorphous phase, which potentially may change its properties, it is necessary to precisely measure the weight percentage of this 'invisible' phase. From the real weight of the sample, m_{Sample}, crystalline standard, m_{St}, and its amount, $\omega_{XRD}(St)$, calculated by (4), we can determine the weight percentage of the amorphous phase, $\omega_{Am} = 100\,\% \cdot m_{Am}/m_{total}$:

$$\omega_{real}(St) = \frac{m_{St}}{m_{St} + m_{Sample}} \cdot 100\% \tag{5}$$

$$\frac{\omega_{Am}}{100\%} = \frac{m_{Am}}{m_{Sample}} = 1 + \frac{m_{St}}{m_{Sample}} \cdot \left(1 - \frac{100\%}{\omega_{XRD}(St)}\right) \tag{6}$$

The details of the calculations with the estimated deviations are presented in the SI, ch. 1.

Some of the fundamental causes of errors in all RIR-based methods are the differences in scattering factors, absorbance, fluorescence, etc. between the sample and standard material. Therefore, we must be careful when choosing the crystalline standard, the applicability of which must be discussed. Another error source in these methods is poor peak and background fitting, caused both by peak overlapping and imperfection of the fitting parameters. Briefly, we must choose the crystalline standard with an RIR value close to the RIR of the sample and a low overlap between the strong peaks of the sample and standard.

To reduce these errors and confirm the results, it is possible to use the method of additives. We can measure every sample a few times with the addition of different amounts of the amorphous sample or crystalline standard to the initial sample/standard mixture. This method is described as the method of additives, applied to multi-peaks realization of Jensen's method [15] for arbitrary standards.

For this, we prepared at least five mixtures of each sample and the silicon standard powder, with Si weight percentages ranging from 2.6% to 50%. We then measured the XRD patterns and performed le Bail fitting of these patterns to measure the integral intensities of the peaks for anatase and silicon. The diffraction patterns for the mixture between titania samples and Si are exemplified in the SI, Fig. SI1.

In the case of crystalline additives, before calculating the real ω_{Am}, we needed to ensure that there were no significant effects caused by differences in the X-ray absorbances of the standard and the sample. This means that we should check the absence of correlations between $\omega_{real}(St)$ and ω_{Am}. From the profile analysis of the obtained patterns, we calculated the mean integral intensity of silicon for each mixture, then the amount of amorphous phase by Eq. (6), and plotted the calculated ω_{Am} against the added ω_{Si}, as shown in Fig. 3b for the $mTiO_2$ sample. Here, we can observe all the data and check the slope coefficient, which should be within the error range, and examine if any data significantly deviates from the mean value. There is indeed one point in Fig. 3b with the ω_{Si} value close to 0, which can be omitted from further evaluation. Subsequently, we can average the overall ω_{Am} and calculate the standard deviation; in our case, it is 38% ±4 %. A more advanced method is to rewrite Eq. (6) as

$$\frac{100\%}{\omega_{XRD}(St)} = \left(1 - \frac{\omega_{Am}}{100\%}\right) \cdot \frac{m_{Sample}}{m_{St}} + 1 \tag{7}$$

and plot the obtained data as $1/\omega_{XRD}(St)$ vs. m_{Sample}/m_{St} (Fig. 3c). After that, it is possible to determine $\bar{\omega_{Am}}$ from the linearization coefficient with the use of an additional reference point (0, 1), where $m_{Sample} = 0$ and $\omega_{XRD}(St) = 1$. The linear fit in this representation, using errors as weight coefficients, yields a slope coefficient of 0.617 ± 0.007, therefore $\bar{\omega_{Am}} = 38.3\% \pm 0.7\%$ and with respect to the previously calculated $\omega_{Brookite} = 13.5\%$, we finally obtain $\omega_{Am} = 30\% \pm 1\,\%$. Fixing of the intercept value does not significantly change the results in the case of the uniform distribution of ω_{Am} against ω_{Si}, but it may be useful when there is insufficient data. Data from other samples obtained by this method are shown in Table 2.

To demonstrate the consistency of this method, we added different weights of amorphous TiO_2 to $mTiO_2$ and measured the total amount of XRD-amorphous phase in each mixture. The results are plotted in Fig. 3d. The linear fit of the data at this scale sets the intercept value equal to the XRD-amorphous content in the initial sample; in our case it is 36% ±2 %. The obtained value is very close to the previously calculated value of 38.3% ±0.7 %, hence we can be sure of the consistency of this method.

Finally, we must emphasize that the calculated $\bar{\omega_{Am}}$ includes amounts of adsorbed gases and H_2O, and it is always necessary to consider the thermal analysis data.

3.5. IR and thermogravimetry data analysis

The IR spectrum of the P25 sample is exemplified in Fig. 2. This spectrum contains two types of OH-related bands, which are also typical for the spectra of other samples. The first band (wide band at 3316 cm^{-1}) corresponds to stretching vibrations of physically adsorbed water molecules [48–51]. The second band (narrow bands at 3630, 3660, and 3690 cm^{-1}) can be attributed to free or hydrogen bonded —OH groups on the surface of crystalline titania [48–58]. Using IR spectroscopy, the presence of water and the absence of organics are verified, hence, in this case we can use thermogravimetry to distinguish different types of adsorbed water.

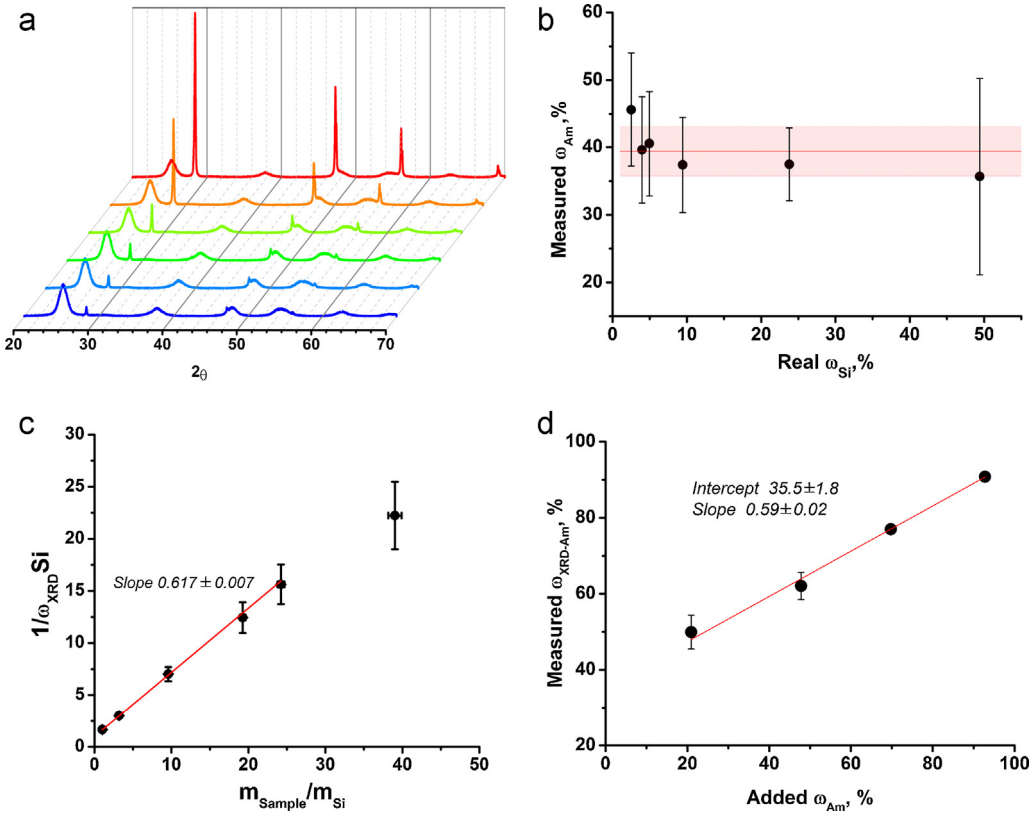

Fig. 3. (a) XRD patterns of Si and mTiO$_2$ sample mixtures, (b) calculated ω_{Am} vs. Si amount without correction to the brookite presence, mean value with deviation labeled with a straight line, (c) graph for calculation $\omega_{\tilde{A}m}$ by linear fit, and (d) measured amorphous phase amount against the added.

To estimate the amount of amorphous titania, we calculated the amount of physisorbed water, which did not significantly influence the measured PCA. It should be noted that insofar as chemically adsorbed water is the part of titania oxohydroxides, so-called 'amorphous titania', and we must distinguish between these two forms of water.

The simplest method is to define the temperature at which we expect full removal of physisorbed water and elimination of chemisorbed water to commence. However, in the case of mesoporous materials, first, this temperature will be different for different samples. Second, the temperature of physisorbed water removal increases and these two processes may overlap. To distinguish these, we plot the first derivative of TG graph (Fig. 4). The first negative peak corresponds to the removal of physisorbed water, therefore, the discrimination temperature was chosen as the endpoint of this peak, which is about ~130 °C. The results of these measurements and the calculated amounts of amorphous titania without physisorbed water are shown in Table 2.

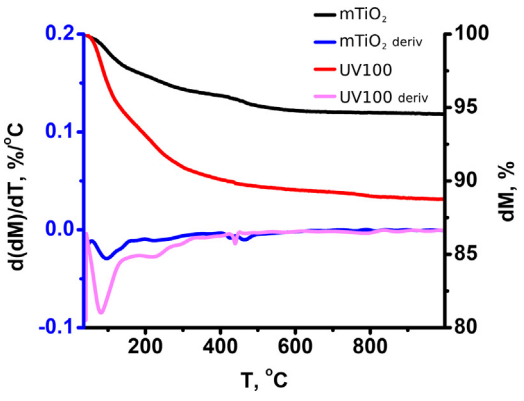

Fig. 4. Thermographs and its first derivatives for UV100 and mTiO$_2$ samples.

3.6. Processing of samples for removing the amorphous phase

To remove the amorphous portion of TiO$_2$, two different approaches were used. The first is based on the crystallization of amorphous TiO$_2$ during annealing at temperatures higher than 400 °C. The complexities of this approach are phase transitions in already crystalline titania and agglomeration of TiO$_2$ particles with the decrease in SSA. Both effects may significantly affect the measured PCA of the samples. To consider this, we performed two series of sample annealing at the same temperatures, (400 °C, 500 °C, 600 °C, and 700 °C). The first series used a heating rate of 5 °C/min with 3 h of annealing, whereas the second series used fast annealing since the sample was placed in a hot oven for 15 min. The phase transitions in all of the samples were measured by XRD. The SSA changes were measured by multipoint BET. The rutile phase is observed in the samples obtained by slow heating to 500 °C and higher, and by fast heating to 600 °C and higher. The SSA decreases dramatically with the annealing temperature, from the initial value of 150 m^2/g to 60 m^2/g for the 'fast' 500 °C-sample. At the same time, the CSR of the anatase phase increases to 55 ± 5 nm (Fig. SI6). Therefore, due to the significant impact of the phase composition on the measured PCA, for the final comparison with commercial TiO$_2$, we used only the samples annealed at 400 °C and 500 °C using fast heating. The phase compositions, CSR, SSA, and PCA data for all the samples are shown in SI, ch. 5 with brief descriptions, as well as partially in Table 2.

Annealing of the commercial UV100 sample was performed at 400 °C and 500 °C using the fast heating method. The SSA of the

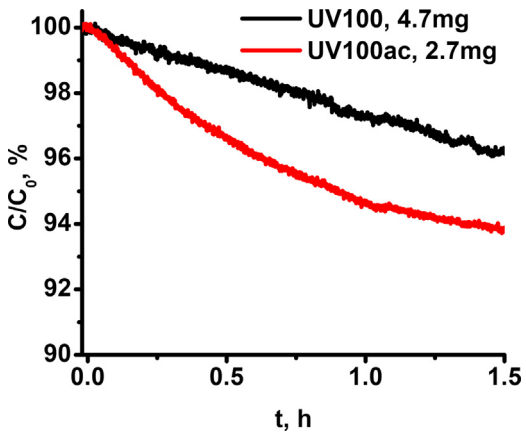

Fig. 5. Comparison of MO decoloration rates in the presence of UV100 catalyst before and after acidifying.

annealed samples decreases simultaneously with the percentage of amorphous phase, and the PCA of these samples significantly increases (Table 2).

As discussed earlier, in the case of thermoprocessing titania samples, the PCA may change for various reasons. To reduce these changes, we suggest using soft chemistry methods for removal of the amorphous phase. The second approach was based on different dissolution rates of different titania phases, particularly, on the fast dissolution of amorphous titania in acids. In the case of TiO_2, we can selectively remove amorphous titania from samples by exposure to diluted nitric acid for a relatively short time. For that process, a portion of the TiO_2 sample was added to 1 M HNO_3, stirred for 3 h, centrifuged and washed with distilled water at least 3 times, then dried at 60 °C. Minor remnants of nitric acid would not change the measured PCA because all photocatalytic measurements were performed in the buffer solution (pH 6.9). The time dependencies of the dye concentration in the presence of the initial and acidified UV100 are shown in Fig. 5. The acidified UV100 sample has a significantly higher PCA than the source UV100. This may explain the high PCA of the UV100 sample measured in acids [19].

Both methods decrease the amorphous titania amount after treatment and significantly increase the PCA of the titania sample.

3.7. *Photocatalytic activity of initial and processed samples*

Different mechanisms for azo-dye decoloration are well-known, both under aerobic and anaerobic conditions [40,59–62]. The relatively slow reaction (a few hours for 50% decoloration) and the contact between the mixture and air during the circulation indicate that the process in our setup is aerobic. It is known that under aerobic conditions at pH 6.9, oxygen is reduce more rapidly, than the unprotonated dye [59]. To confirm the oxidative nature of the reaction, additional experiments were performed. Aerating the mixture by air flow leads to an increase in the decoloration rate, but bubbling with nitrogen decreases it. The details are presented in the SI (ch. 6).

The presence of reaction products, as described in [63], may reduce the observable reaction rate, but it was shown in [40] that for such concentration of MO a difference between the observable and expected constants of reaction less than 15% at the time of 50% decoloration $t_{1/2}$. Therefore, since the rate was calculated based on the first hour and the decoloration at this time is ~20%, the difference between the real and observed rates is low enough to use this process for comparison of titania catalysts.

The rate of MO decoloration under UV illumination without a catalyst was low enough to be neglected (<1 %/*h*).

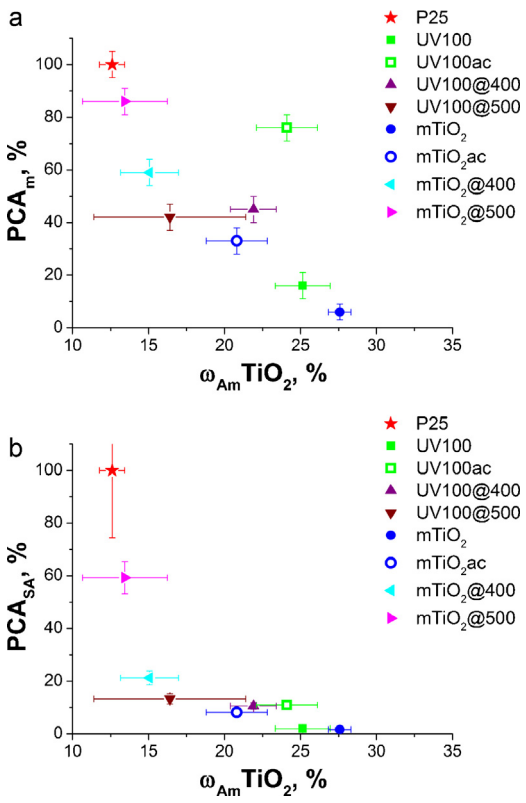

Fig. 6. (a) Dependence of photocatalytic activity, normalized on the sample weight vs. amorphous titania amount. (b) Dependence of photocatalytic activity, normalized on the sample surface area *vs.* amorphous titania amount.

According to the BET surface area calculations, the amTiO$_2$ sample has a high SSA of 250 m^2/g. It is worth mentioning that due to the high surface area and significant amount of defects, amorphous TiO_2 readily adsorbs water and other molecules and may have OH-groups on the surface as well, but this sample exhibits negligible PCA. The observed MO decoloration rate is in the range of MO decoloration under UV without a catalyst. A comparison of the SSA and PCA values of the same samples in Table 2 demonstrates that the anatase samples with high SSA, such as the initial UV100 and mesoporous TiO_2, have an extremely low PCA.

It is assumed that this effect is caused by the presence of the amorphous phase, which was detected by TEM and quantitatively measured by XRD. To confirm this, we plotted the PCA vs. $\omega_{Am}TiO_2$ for all partially crystallized samples (Fig. 6a). Here, the PCA is shown normalized to the weight of the sample, as is the common form; however, due to the different nature of the samples and, hence, the different SSAs, it seems reasonable to plot PCA normalized to the SSA of the samples (Fig. 6b).

It was demonstrated that fast annealing of titania at 400 °C and 500 °C leads to decreases in the amorphous phase percentage and increases in the PCA. Even small changes in ω_{Am} and SSA may result in strong increases of the PCA, e.g. in the case of acidifying UV100. This effect is probably due to changes in the spatial distribution of the amorphous phase. Therefore, the influence of the amorphous phase spatial distribution on PCA should be investigated in the future.

4. Conclusions

In this work we demonstrate that the presence of the amorphous $TiO_{2-0.5n}(OH)_n \cdot xH_2O$ phase may directly affect the PCA. Furthermore, the importance of quantitative measurements of the amorphous phase amount for correct studies of titania-based

catalysts and composites was demonstrated. The proposed method for the quantitative analysis of the XRD-amorphous phase allows one to measure the weight percent of the XRD-amorphous titanium oxohydroxides fraction with high accuracy. According to the obtained data, the samples containing a higher amount of the amorphous phase show a lower PCA, as measured in an aerobic aqueous solution with neutral pH. It was demonstrated that partial removal of the amorphous phase leads to significant increases in the PCA. The results of the amorphous phase removal experiments using acids may explain the high PCA of titania samples with a high amount of amorphous phase (e.g. Hombikat UV100) obtained when measured in acidic media.

Acknowledgements

This work was supported by RFBR (research project No. 15-03-99537a), Euler program of DAAD (2011), and M.V. Lomonosov Moscow State University Program of Development. The authors would like to thank PhD P.V. Evdokimov (Faculty of Materials Science, Lomonosov Moscow State University) for the thermogravimetric experiments and Kh.E. Yorov (Faculty of Materials Science, Lomonosov Moscow State University) for the SSA measurements of the annealed mTiO_2 samples.

Appendix A. Supplementary data

Supplementary data associated with this article can be found, in the online version, at http://dx.doi.org/10.1016/j.apcatb.2016.05.010.

References

[1] M. Kaneko, I. Okura, Photocatalysis: Science and Technology, Kodansha and Springer, New York, 2002.
[2] O. Carp, C. Huisman, A. Reller, Photoinduced reactivity of titanium dioxide, Prog. Solid State Chem. 32 (1–2) (2004) 33–177.
[3] L. Saadoun, J. Ayllón, J. Jiménez-Becerril, J. Peral, X. Domènech, R. Rodríguez-Clemente, 1,2-Diolates of titanium as suitable precursors for the preparation of photoactive high surface titania, Appl. Catal. B: Environ. 21 (4) (1999) 269–277.
[4] K.L. Yeung, S.T. Yau, A. Maira, J.M. Coronado, J. Soria, P.L. Yue, The influence of surface properties on the photocatalytic activity of nanostructured TiO_2, J. Catal. 219 (1) (2003) 107–116.
[5] A.D. Paola, M. Bellardita, L. Palmisano, Z. Barbieriková, V. Brezová, Influence of crystallinity and {OH} surface density on the photocatalytic activity of TiO_2 powders, J. Photochem. Photobiol. A: Chem. 273 (0) (2014) 59–67.
[6] J.M. Coronado, A.J. Maira, J.C. Conesa, K.L. Yeung, V. Augugliaro, J. Soria, EPR study of the surface characteristics of nanostructured TiO_2 under UV irradiation, Langmuir 17 (17) (2001) 5368–5374.
[7] A. Maira, K. Yeung, J. Soria, J. Coronado, C. Belver, C. Lee, V. Augugliaro, Gas-phase photo-oxidation of toluene using nanometer-size TiO_2 catalysts, Appl. Catal. B: Environ. 29 (4) (2001) 327–336.
[8] T. Hathway, W.S. Jenks, Effects of sintering of TiO_2 particles on the mechanisms of photocatalytic degradation of organic molecules in water, J. Photochem. Photobiol. A: Chem. 200 (2–3) (2008) 216–224.
[9] M. Anpo, T. Shima, S. Kodama, Y. Kubokawa, Photocatalytic hydrogenation of propyne with water on small-particle titania: size quantization effects and reaction intermediates, J. Phys. Chem. 91 (16) (1987) 4305–4310.
[10] A. Maira, K. Yeung, C. Lee, P. Yue, C. Chan, Size effects in gas-phase photo-oxidation of trichloroethylene using nanometer-sized TiO_2 catalysts, J. Catal. 192 (1) (2000) 185–196.
[11] X. Wang, L. Sø, R. Su, S. Wendt, P. Hald, A. Mamakhel, C. Yang, Y. Huang, B.B. Iversen, F. Besenbacher, The influence of crystallite size and crystallinity of anatase nanoparticles on the photo-degradation of phenol, J. Catal. 310 (0) (2014) 100–108, Special issue on Photocatalysis and Photoelectrolysis.
[12] M.A. Henderson, A surface science perspective on photocatalysis, Surf. Sci. Rep. 66 (6–7) (2011) 185–297.
[13] B. Ohtani, Y. Ogawa, S. Nishimoto, Photocatalytic activity of amorphous-anatase mixture of titanium(IV) oxide particles suspended in aqueous solutions, J. Phys. Chem. B 101 (19) (1997) 3746–3752.
[14] M. Inagaki, Y. Nakazawa, M. Hirano, Y. Kobayashi, M. Toyoda, Preparation of stable anatase-type TiO_2 and its photocatalytic performance, Int. J. Inorg. Mater. 3 (7) (2001) 809–811.
[15] H. Jensen, K. Joensen, J.-E. Jørgensen, J. Pedersen, G. Søgaard, Characterization of nanosized partly crystalline photocatalysts, J. Nanoparticle Res. 6 (5) (2004) 519–526.
[16] B. Ohtani, O. Prieto-Mahaney, D. Li, R. Abe, What is Degussa (Evonik) P25? Crystalline composition analysis, reconstruction from isolated pure particles and photocatalytic activity test, J. Photochem. Photobiol. A: Chem. 216 (2–3) (2010) 179–182, 3rd International Conference on Semiconductor Photochemistry, SP-3, April, 2010, Glasgow, UK.
[17] D. Tobaldi, R. Pullar, M. Seabra, J. Labrincha, Fully quantitative X-ray characterisation of Evonik Aeroxide TiO_2 P25(r), Mater. Lett. 122 (0) (2014) 345–347.
[18] M. Gratzel, Properties and Applications of Nanocrystalline Electronic Junctions, 2000, pp. 527–553.
[19] K. Tanaka, M.F. Capule, T. Hisanaga, Effect of crystallinity of TiO_2 on its photocatalytic action, Chem. Phys. Lett. 187 (1–2) (1991) 73–76.
[20] M. Crocker, R.H.M. Herold, A.E. Wilson, M. Mackay, C.A. Emeis, A.M. Hoogendoorn, ^{1}H NMR spectroscopy of titania. Chemical shift assignments for hydroxy groups in crystalline and amorphous forms of TiO_2, J. Chem. Soc. Faraday Trans. 92 (1996) 2791–2798.
[21] V. Sepelak, A. Duvel, M. Wilkening, K.-D. Becker, P. Heitjans, Mechanochemical reactions and syntheses of oxides, Chem. Soc. Rev. 42 (2013) 7507–7520.
[22] L.S. Hsu, R. Rujkorakarn, J.R. Sites, C.Y. She, Thermally induced crystallization of amorphous-titania films, J. Appl. Phys. 59 (10) (1986) 3475–3480.
[23] C. Chao, Z. Ren, S. Yin, G. Xu, S. Gong, X. Yang, X. Li, G. Shen, G. Han, Dissolution/recrystallization growth of titanate nanostructures by amorphous precursor, Adv. Powder Technol. 25 (2) (2014) 745–751.
[24] C. Colbeau-Justin, M. Kunst, D. Huguenin, Structural influence on charge-carrier lifetimes in TiO_2 powders studied by microwave absorption, J. Mater. Sci. 38 (11) (2003) 2429–2437.
[25] D.C. Hague, M.J. Mayo, Controlling crystallinity during processing of nanocrystalline titania, J. Am. Ceram. Soc. 77 (7) (1994) 1957–1960.
[26] G. Bertoni, E. Beyers, J. Verbeeck, M. Mertens, P. Cool, E. Vansant, G.V. Tendeloo, Quantification of crystalline and amorphous content in porous samples from electron energy loss spectroscopy, Ultramicroscopy 106 (7) (2006) 630–635.
[27] S.S. Gorelik, Y.A. Skakov, L.N. Rastorguev, Rentgenograficheskii i elektronno-opticheskii analiz (X-ray Diffraction and Electron-Optical Analysis), Inst. Stali i Splavov, Moscow, 1994 (in Russian).
[28] H. Zhang, J.F. Banfield, Kinetics of crystallization and crystal growth of nanocrystalline anatase in nanometer-sized amorphous titania, Chem. Mater. 14 (10) (2002) 4145–4154.
[29] V. Petkov, G. Holzhüter, U. Tröge, T. Gerber, B. Himmel, Atomic-scale structure of amorphous TiO_2 by electron, X-ray diffraction and reverse Monte Carlo simulations, J. Non-Cryst. Solids 231 (1–2) (1998) 17–30.
[30] H. Zhang, B. Chen, J.F. Banfield, G.A. Waychunas, Atomic structure of nanometer-sized amorphous TiO_2, Phys. Rev. B 78 (Dec 2008) 214106.
[31] K. Kaur, S. Prakash, N. Goyal, R. Singh, P. Entel, Structure factor of amorphous TiO_2 nanoparticle; molecular dynamics study, J. Non-Cryst. Solids 357 (19–20) (2011) 3399–3404.
[32] V. Van Hoang, Structural properties of simulated liquid and amorphous TiO_2, Phys. Status Solidi (b) 244 (4) (2007) 1280–1287.
[33] M. Landmann, T. Köhler, S. Köppen, E. Rauls, T. Frauenheim, W.G. Schmidt, Fingerprints of order and disorder in the electronic and optical properties of crystalline and amorphous TiO_2, Phys. Rev. B 86 (August) (2012) 064201.
[34] J. Livage, M. Henry, C. Sanchez, Sol–gel chemistry of transition metal oxides, Prog. Solid State Chem. 18 (4) (1988) 259–341.
[35] J.M. Kim, Y.-J. Han, B.F. Chmelka, G.D. Stucky, One-step synthesis of ordered mesocomposites with non-ionic amphiphilic block copolymers: implications of isoelectric point, hydrolysis rate and fluoride, Chem. Commun. (2000) 2437–2438.
[36] E.A. Smirnov, M.A. Meledina, A.V. Garshev, V.I. Chelpanov, S. Frost, J.U. Wieneke, M. Ulbricht, Grafting of titanium dioxide microspheres with a temperature-responsive polymer via surface-initiated atom transfer radical polymerization without the use of silane coupling agents, Polym. Int. 62 (5) (2013) 836–841.
[37] N.N. Gracheva, A.Y. Romanchuk, E.A. Smirnov, M.A. Meledina, A.V. Garshev, E.A. Shirshin, V.V. Fadeev, S.N. Kalmykov, Am(III) sorption onto TiO_2 samples with different crystallinity and varying pore size distributions, Appl. Geochem. 42 (2014) 69–76.
[38] D. Nečas, P. Klapetek, Gwyddion: an open-source software for SPM data analysis, Central Eur. J. Phys. 10 (2012) 181–188.
[39] V.A. Lebedev, V.V. Sudin, D.A. Kozlov, A.V. Garshev, Photocatalytical properties of nanocrystalline TiO_2, modified with CuO and WO_3, Nanotechnol. Russia 11 (2016) 20–28.
[40] N. Guettaï, H.A. Amar, Photocatalytic oxidation of methyl orange in presence of titanium dioxide in aqueous suspension. Part II: kinetics study, Desalination 185 (1–3) (2005) 439–448, Desalination and the Environment.
[41] D. Monllor-Satoca, R. Gómez, M. Gonzáez-Hidalgo, P. Salvador, The "Direct-Indirect" model: an alternative kinetic approach in heterogeneous photocatalysis based on the degree of interaction of dissolved pollutant species with the semiconductor surface, Catal. Today 129 (1–2) (2007) 247–255, Selected Contributions of the 4th European Meeting on Solar Chemistry and Photocatalysis: Environmental Applications (SPEA 4).
[42] Y. Li, X. Li, J. Li, J. Yin, Photocatalytic degradation of methyl orange by TiO_2-coated activated carbon and kinetic study, Water Res. 40 (6) (2006) 1119–1126.
[43] S. Al-Qaradawi, S.R. Salman, Photocatalytic degradation of methyl orange as a model compound, J. Photochem. Photobiol. A: Chem. 148 (1–3) (2002) 161–168.
[44] V. Petricek, M. Dusek, L. Palatinus, Crystallographic Computing System JANA2006: General features, Z. Kristallogr. – Cryst. Mater. 229 (May) (2014) 345–352.
[45] V.K. Pecharsky, P.Y. Zavalij, Fundamentals of Powder Diffraction and Structural Characterisation of Materials, Springer, New York, 2005.

[46] L.W. Finger, D.E. Cox, A.P. Jephcoat, A correction for powder diffraction peak asymmetry due to axial divergence, J. Appl. Crystallogr. 27 (December) (1994) 892–900.
[47] A.L. Bail, H. Duroy, J. Fourquet, Ab-initio structure determination of LiSbWO6 by X-ray powder diffraction, Mater. Res. Bull. 23 (3) (1988) 447–452.
[48] Y. Suda, T. Morimoto, Molecularly adsorbed water on the bare surface of titania (rutile), Langmuir 3 (5) (1987) 786–788.
[49] P. Jones, J.A. Hockey, Infra-red studies of rutile surfaces. Part 2. Hydroxylation, hydration and structure of rutile surfaces, Trans. Faraday Soc. 67 (1971) 2679–2685.
[50] D.M. Griffiths, C.H. Rochester, Infrared study of the adsorption of water on to the surface of rutile, J. Chem. Soc. Faraday Trans. 1 73 (1977) 1510–1529.
[51] G. Munuera, F.S. Stone, Adsorption of water and organic vapours on hydroxylated rutile, Discuss. Faraday Soc. 52 (1971) 205–214.
[52] W. Li, D. Li, Y. Lin, P. Wang, W. Chen, X. Fu, Y. Shao, Evidence for the active species involved in the photodegradation process of methyl orange on TiO_2, J. Phys. Chem. C 116 (5) (2012) 3552–3560.
[53] W. Li, D. Du, T. Yan, D. Kong, J. You, D. Li, Relationship between surface hydroxyl groups and liquid-phase photocatalytic activity of titanium dioxide, J. Colloid Interface Sci. 444 (2015) 42–48.
[54] D.J.C. Yates, Infrared studies of the surface hydroxyl groups on titanium dioxide, and of the chemisorption of carbon monoxide and carbon dioxide, J. Phys. Chem. 65 (5) (1961) 746–753.
[55] K.E. Lewis, G.D. Parfitt, Infra-red study of the surface of rutile, Trans. Faraday Soc. 62 (1966) 204–214.
[56] K. Tanaka, J.M. White, Characterization of species adsorbed on oxidized and reduced anatase, J. Phys. Chem. 86 (24) (1982) 4708–4714.
[57] M. Primet, P. Pichat, M.V. Mathieu, Infrared study of the surface of titanium dioxides. I. Hydroxyl groups, J. Phys. Chem. 75 (9) (1971) 1216–1220.
[58] K. Takahashi, H. Yui, Analysis of surface OH groups on TiO_2 single crystal with polarization modulation infrared external reflection spectroscopy, J. Phys. Chem. C 113 (47) (2009) 20322–20327.
[59] G.T. Brown, J.R. Darwent, Photoreduction of methyl orange sensitized by colloidal titanium dioxide, J. Chem. Soc. Faraday Trans. 1 80 (1984) 1631–1643.
[60] J. Peral, A. Mills, Factors affecting the kinetics of methyl orange reduction photosensitized by colloidal CdS, J. Photochem. Photobiol. A: Chem. 73 (1) (1993) 47–52.
[61] I.K. Konstantinou, T.A. Albanis, TiO_2-assisted photocatalytic degradation of azo dyes in aqueous solution: kinetic and mechanistic investigations: a review, Appl. Catal. B: Environ. 49 (1) (2004) 1–14.
[62] A. Mills, J. Wang, Photobleaching of methylene blue sensitised by TiO_2: an ambiguous system? J. Photochem. Photobiol. A: Chem. 127 (1–3) (1999) 123–134.
[63] C. Baiocchi, M.C. Brussino, E. Pramauro, A.B. Prevot, L. Palmisano, G. Marc, Characterization of methyl orange and its photocatalytic degradation products by HPLC/UV-VIS diode array and atmospheric pressure ionization quadrupole ion trap mass spectrometry, Int. J. Mass Spectrom. 214 (2) (2002) 247–256.